Eur. Phys. J. A (2023) 59:36
https://doi.org/10.1140/epja/s10050-023-00945-5

THE EUROPEAN PHYSICAL JOURNAL A

Regular Article - Experimental Physics

Neutron capture cross section of ^{83}Kr

Stefan Fiebiger[1], Bayarbadrakh Baramsai[2], Aaron Couture[2], Milan Krtička[3], Shea Mosby[2], John O'Donnell[2], René Reifarth[1,4,a], Gencho Rusev[2], John Ullmann[2], Mario Weigand[1], Clemens Wolf[1]

[1] Goethe University Frankfurt, Max-von-Laue Str. 1, Frankfurt 60438, Germany
[2] Los Alamos National Laboratory, Los Alamos 87545, USA
[3] Charles University, Prague, Czech Republic
[4] University of Notre Dame, Notre Dame 46556, IN, USA

Received: 15 October 2022 / Accepted: 2 February 2023

Communicated by Nicolas Alamanos

Abstract The neutron capture cross section of ^{83}Kr has been measured via the time-of-flight technique between 25 meV and 500 keV. The experiment used the DANCE array at the Los Alamos National Laboratory. Maxwellian Averaged Cross Sections have been derived for a range of stellar temperatures and are found to be in good agreement with previous data. The impact of the new cross sections on stellar nucleosynthesis has been investigated.

1 Introduction

Nearly all elements heavier than iron are produced in a neutron induced process. The two major processes are the r process (rapid) and the s process (slow) which differ mainly by neutron density and duration. While the range for neutron density during the s process is $10^8 < \frac{n_n}{\mathrm{cm}^{-3}} \leq 10^{12}$ with exposure times upto thousands of years, the neutron density during the r process is $10^{20} < \frac{n_n}{\mathrm{cm}^{-3}} \leq 10^{22}$ lasting only for a few seconds [1,2]. Only a few isotopes on the proton-rich side of the valley of stability get significant contributions from other processes like the γ-process [3–5].

About 50% of the elements beyond strontium are produced during the main component of the s-process, which takes place in thermally pulsing Red Giant stars (TP-AGB). These stars have left the main sequence after finishing hydrogen core burning. They are about 50–100 times bigger and cooler than our sun while their masses are between 3 and 9 solar masses [6]. In the classical picture, the s-process starts with an iron seed exposed to free neutrons. Since the neutron densities are low, an unstable isotope produced by a series of neutron capture reactions will almost always β-decay back to its stable isobar before capturing another neutron. Thus, the s-process builds up the elements following the neutron-rich side of the nuclear valley of stability until it terminates in the lead-bismuth region. In the more advanced stellar picture, the seed is more than just iron, but also other elements from previous phases or original composition of the star [7].

If the neutron capture rate is comparable to the β-decay rate a so called branching points exists. This means the s-process path can follow two distinct ways. The branching ratio is hereby depended on the temperature of the star [8,9].

In this paper we report on measurments of the neutron capture cross sections of ^{83}Kr near the branching point ^{85}Kr [10]. The experiment was performed at Los Alamos Neutron Science Center (LANSCE) using the 4πBaF$_2$ Detector for Advanced Neutron Capture Experiments (DANCE) [11]. This allowed using Q-value and multiplicity cuts to discriminate between respective Kr isotope and background events.

2 Samples

2.1 ^{83}Kr sample

Preparation of suitable samples provided a particular challenge. As krypton is a noble gas it exhibits a low freeze-out temperature (120 K at standard pressure), which complicated the filling process of the utilized high pressure stainless steel spheres with a diameter of 10 mm and 0.2 mm wall thickness, see Fig. 1. Further details can be found here [12]. Enriched ^{83}Kr with a purity of 99.933% was used [13]. The total amount of gas in the sphere was 26.12 ± 0.01 mg at a pressure of 13.79 bar. For the use at DANCE a new target holder had to be designed that held the gas sphere at an angle of 61 degrees so only the gas filled spherical top part was inside the neutron beam. The overall length of this target holder design is 66.4 mm and therefore about 18.7 mm

[a] e-mail: reifarth@physik.uni-frankfurt.de (corresponding author)

Published online: 24 February 2023

longer compared to the standard holder that is usually used at DANCE. During the designing special attention was given to the centering of the gas sphere in the detector.

3 Experiment

The experiment to determine the neutron capture cross section for ^{83}Kr was performed at Lujan Neutron Scattering Center at LANL [14]. The facility provides white neutron pulses with a repetition rate of 20 Hz. The neutrons are produced via a spallation reaction triggered by a proton beam impinging a tungsten block with a current of about 100 μA [15,16]. To measure an energy depended cross section the time of flight method was employed, which uses the neutron flight time between production at the spallation target and the (n,γ)-reaction in the detector [17]. With a flight path of 20.28 m it is possible to determine the neutron energy of a reaction.

3.1 Dance

The main instrument to determine the (n,γ) cross section was DANCE. A calorimetric detector composed of 162 elements, whereas two are left out for the beam pipe. The remaining 160 BaF_2 detectors cover a solid angle of 3.5π [18]. This allows the detection of the γ-rays of a cascade following a neutron capture event with very high efficiency. A high detection efficiency allows the discrimination of cneutron captures on different substances within a sample based on the sum of all γ-rays detected, which is close to the reaction Q-value. The detector segmentation was used to further differentiate between capture events on the sample and events caused by scattered neutrons by using the number of responding detectors of an event. Neighboring detectors which have fired were assumed to be a single cluster of detectors and the number of such clusters is referred to as the cluster multiplicity (Mcl) [19]. This which was used in the analysis of the Kr data. The detector sphere formed by the BaF_2 crytals has an inner radius of $r_i = 10.5$ cm and an outer radius of $r_o = 16.5$ cm. Inside this sphere, a ^{6}LiH sphere was placed to significantly suppress events caused by scattered neutrons [19].

The scintallator material BaF_2 contains an intrinsic and unavoidable Ra contamination from the productions process. The subsequent decay of Ra produces signals from the emitted α-particles. These signals can be distinguished from the γ-radiation by taking advantage of the two decay components of BaF_2 with $\tau_{\text{fast}} = 0.6\,\text{ns} - 0.8\,\text{ns}$ and $\tau_{\text{slow}} = 630\,\text{ns}$ where the α-particles almost exclusively excite the slow component. By examining both components a data cut can be employed to remove the signals originating from α-particles (see [18] for details).

3.2 Execution of experiment

^{83}Kr was irradiated for about 3 h in total. To reduce pile-up in the large resonances, the target mass was reduced to 26.12 ± 0.01 mg. Further reduction was not sensible, because of the to resulting poor signal to background ratio. Most of the background originated from neutron interactions with the stainless steel sphere. Instead, the proton current reaching the spallation target was reduced to about 40 μA for 1 h. For the rest of the time allocated to the ^{83}Kr measurement, the full current was used to achieve good statistics in the regions between resonances. A second measurement with an identical empty target sphere and holder was performed to account for background from the detector and the sample.

4 Analysis

4.1 Neutron monitor calibration

The characteristic neutron spectrum, $\Phi(E)$, with the neutron energy E, from the spallation source at LANSCE had to be unfolded from the data to extract the capture cross section, $\sigma(E)$. The general correlation is given by: $\sigma(E) \cdot \Phi(E) = C$, with C the detected counts in the energy bin at E. For this purpose a ^{6}Li beam monitor (BM) was used, which was placed down-stream of the sample, outside the DANCE array. It detects the neutrons via ^{6}Li(n,α). To correct for the difference in flux a factor k_{BM} was introduced so the flux at the sample is given by:

$$\Phi(E) = k_{\text{BM}} \cdot \frac{C_{\text{BM}}}{\sigma_{\text{BM}}(E)} \tag{1}$$

To determine k_{BM} an additional measurement using an Au foil with a thickness of 5000 Å was performed:

$$k_{\text{BM}} = \frac{\varepsilon_{\text{Au}} N_{\text{Au}} \sigma_{\text{Au}}}{C_{\text{Au}}} \frac{C_{\text{BM}}}{\sigma_{\text{BM}}} \tag{2}$$

Here ϵ_{Au} denotes the detector efficiency which was determined with GEANT3 simulations (see Sect. 4.4).

At a neutron energy of 4.89 eV ^{197}Au(n,γ) has a large resonance of 2.74 10^4 b. The measured data were fitted to the evaluated ENDF/B-VII.1 cross section [20]. k_{BM} can then be used for all following Kr measurements.

4.2 Scatter correction

To correct for effects of scattering and absorption in the sample Monte Carlo simulations were performed using the evaluated capture and elastic scatter cross sections. Further parameter were the target geometry and the target density. For every energy step 10^6 neutrons were simulated and their path through the sample tracked and compared to an unscattered

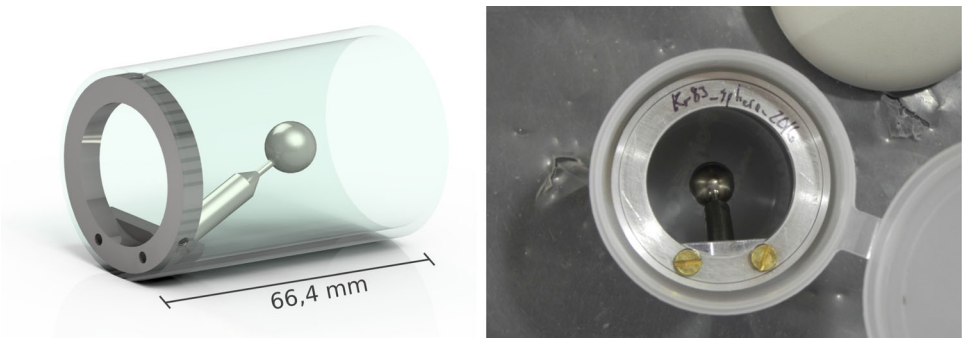

Fig. 1 Left: Computer render of the ^{83}Kr target holder with sample. Right: Front view of the ^{83}Kr target holder with sample

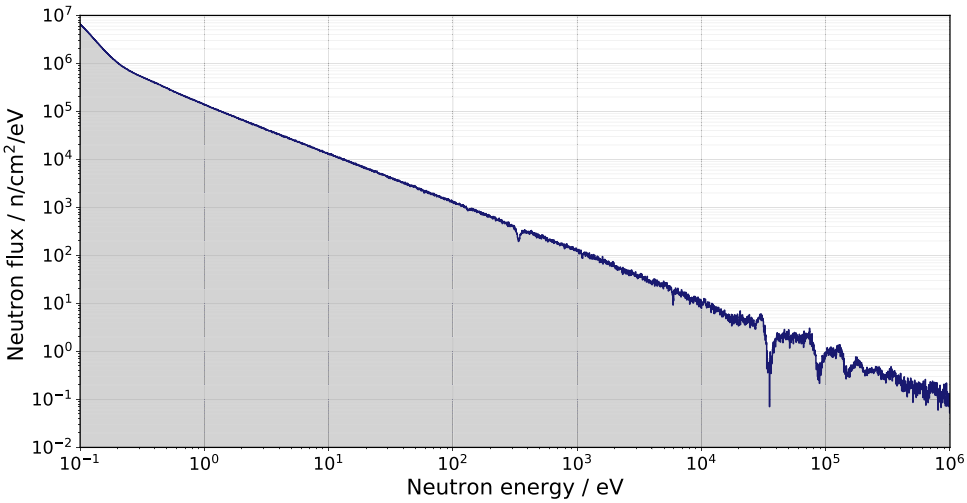

Fig. 2 Normalized spectrum of the ^{6}Li neutron monitor. The reaction used to detect the neutrons was ^{6}Li(n,α)

neutron. In case of low statistics the number of neutrons was increased in certain energy steps to reduce the uncertainty below 0.1%.

4.3 Energy calibration

Energy calibration was achieved using the intrinsic alpha activity of the detector material (see Sect. 3.1). For this method to work the alpha lines of Ra and Po, which is part of Ra decay chain, were initially calibrated with a ^{88}Y γ-source and verified with the same source at the end of the experiment. For every run the energy was then corrected with this γ-calibrated alpha spectrum.

4.4 Efficiency

To determine the correct detector efficiency for specific cuts to Mcl and deposited energy in the detector (E_{sum}) the detector response had to be simulated. For this work GEANT3 [21] simulations were chosen as they were successfully performed before and exhibited good agreement with former measurements [22,23]. First, γ-cascades were created using the tool DICEBOX [24], with these the efficiency could be simulated in GEANT3 using the complete DANCE setup.

4.4.1 DICEBOX

In DICEBOX a level structure is simulated above a critical energy E_{crit} below which all levels with energy, spin and parity are known from measurements. To do this a Monte Carlo approach was chosen which uses, dependent on the simulated nucleus, different models for level density and photon strength functions to create the level structure of the excited nucleus. As it is uncertain which or if a physical model fully describes an excited nucleus, several models were employed. For E1 photon strength functions the Generalized Lorentzian Model [25] was used. For M1 a spin-flip resonance plus low-energy enhancement given by the form $DMG \cdot exp(-E_g/E_{tr})$ and the single-particle model in which the M1 photon strength function is a constant has been used. The single-particle model in which the E2 photon strength function is a constant was chosen for E2. For each set of models 15 realizations with $5 \cdot 10^5$ cascades were simulated whereas a realization is the creation of a nucleus with newly created level structure above E_{crit}.

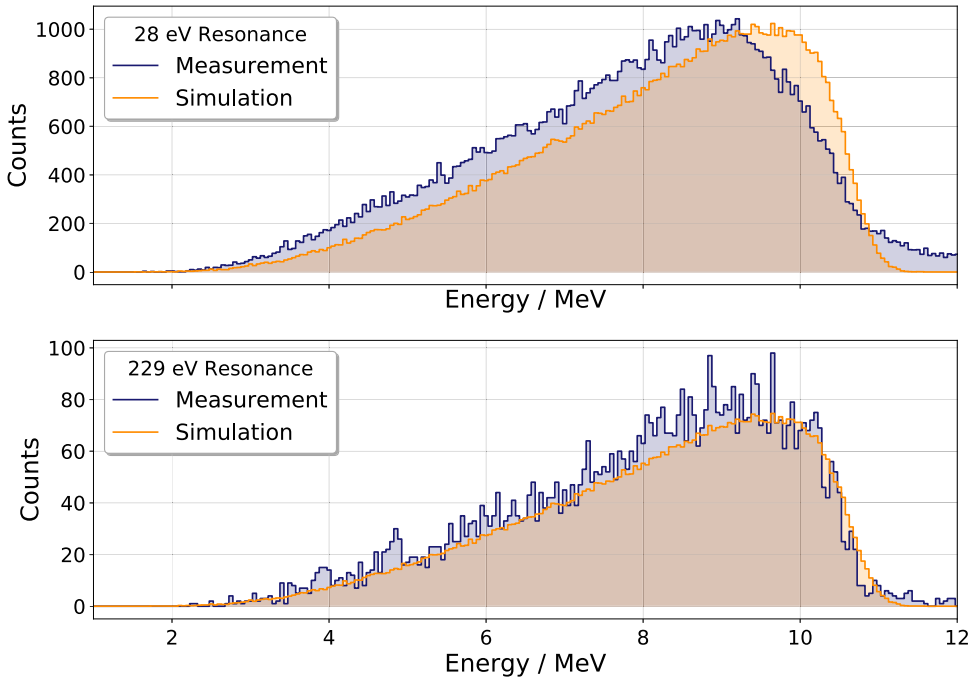

Fig. 3 Comparison of the E_{sum} spectra of the 28 eV and 229 eV resonances with $Mcl = 5$

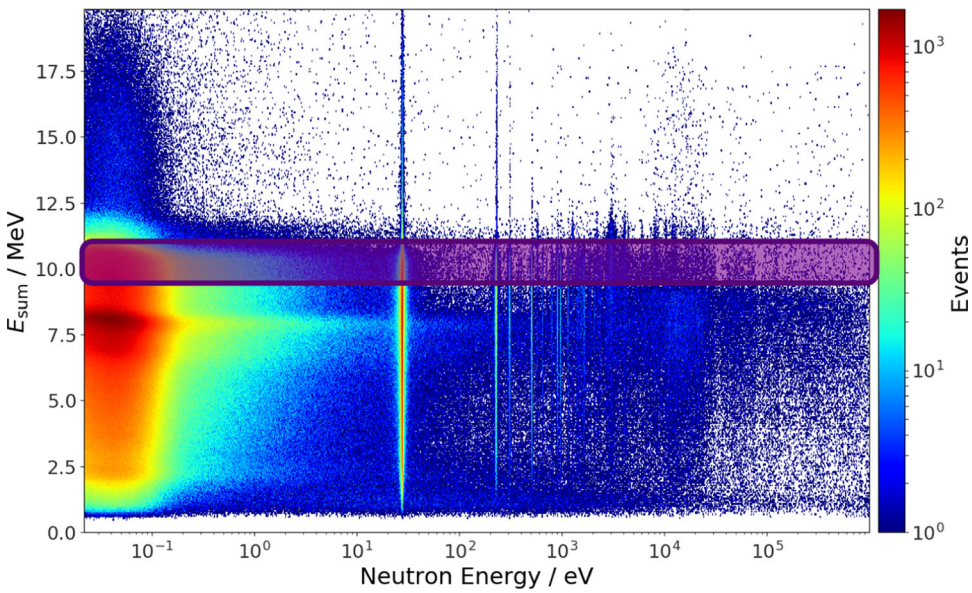

Fig. 4 Two dimensional spectrum of capture events of ^{83}Kr with $Mcl = 3 - 6$. The purple box indicates the cut to E_{sum}

4.4.2 GEANT3

The γ-cascades obtained from DICEBOX were then implemented in the GEANT3-simulation of the DANCE array. The simulation included 160 BaF_2 crystals and the following specifications:

- A spherical crystal mounting made of aluminum.
- A PVC crystal wrapping of about 0.7 mm.
- The photo multiplier tubes glued to the crystals.
- A ^{6}LiH sphere with an inner radius of 10.5 cm and an outer radius of 16.5 cm.
- Two detectors that were mounted but not giving signals.
- The simulations uses the same energy threshold of 150 keV as the data analysis.

^{84}Kr contains a long lived level at 3.24 MeV with a half life of 1.83 μs [26] that occured about 2% of the time. This time is much longer than the coincidence window of 10 ns used for the measurement. To account for this level the cascade from DICEBOX was split and it is expected that in this case only a part of Q-value energy will be deposited in the detector.

The measured E_{sum} spectra show very good agreement with the simulations in the resonances at 229 eV, 314 eV

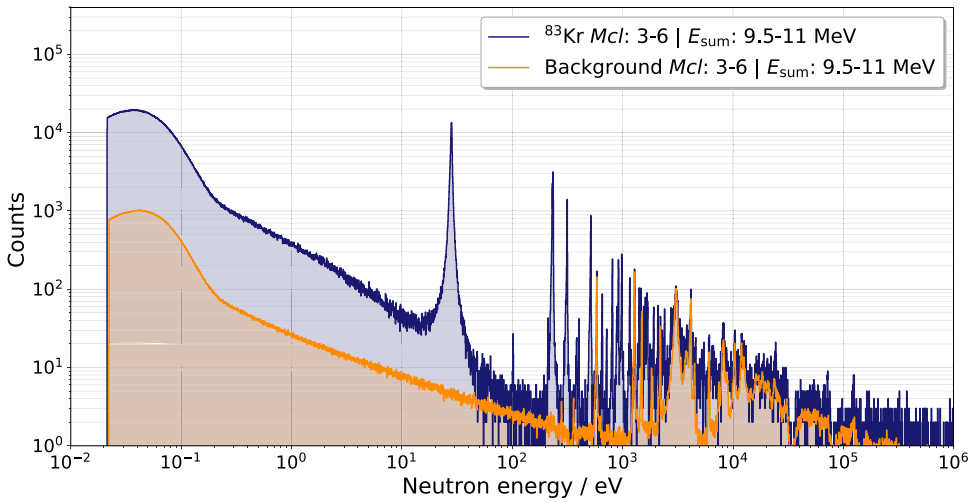

Fig. 5 Number of events in the DANCE detector per neutron energy bin. ^{83}Kr and background spectra are normalized to the same charge on the spallation target

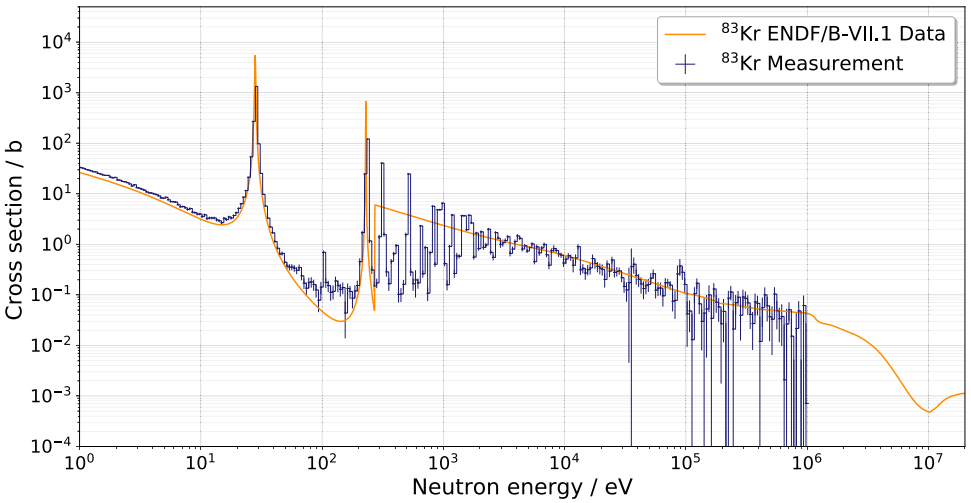

Fig. 6 ^{83}Kr neutron capture cross section with statistical uncertainties. The number of bin is 50 per energy decade. For comparison the evaluated ENDF/B-VII.1 cross section is also displayed

and 513 eV. However at the resonace at 28 eV simulations show larger discrepancies. The measured data show a shift to lower energies of the Q-value peak that cannot be reproduced with the simulations (see Fig. 3). In this energy range larger systematic uncertainties had to be taken into account.

The efficiency to detect a ^{83}Kr(n,γ) event was calculated to 0.160 ± 0.004 if the same cuts on deposited energy and cluster multiplicity are applied as for the experimental data (see next section).

4.5 Cuts

The two dimensional spectrum measured with DANCE is shown in Fig. 4. These include a cut on the cluster mulciplicity Mcl. For ^{83}Kr an analysis of the Mcl distribution showed only a small amount of events with $Mcl = 1$ or $Mcl = 2$. As these contain overproportionally many events from scattered neutrons as well, they were not used for further analysis. The spectrum showed further events with Q-values other than the main Kr constituents. In the case of ^{83}Kr(n,γ), with a Q-value of 10.52 MeV [20], this is mainly from the target sphere and holder as well as from the most common Ba isotopes $134 < A < 138$. The high Q-value of ^{83}Kr(n,γ) allowed for a energy cut $E_{sum} = 9.5$–11 MeV removing almost all beam-related background events.

5 Results

5.1 ^{83}Kr cross section

To account for the high count rates in the resonances at 28 eV and 229 eV the sample was measured twice (see Sect. 3.2). The 40 µA measurement reduced pile-up in those resonances while the second 100 µA measurement collected enough statistics in the in regions between the resonances. Both measurements were then combined using Eq. 3.

$$N_f = \frac{N_{b,1} + \frac{N_{p,1}}{N_{p,2}} \cdot N_{b,2}}{2} \tag{3}$$

Table 1 Calculated MACS in this work

kT/keV	MACS(KADoNIS v0.3)/mb	MACS (This work)/mb
5	902.0	$870.8 \pm 13.0_{\text{stat}} \pm 61.5_{\text{sys}}$
10	600.0	$553.5 \pm 14.9_{\text{stat}} \pm 39.1_{\text{sys}}$
15	406.0	$422.0 \pm 17.1_{\text{stat}} \pm 29.8_{\text{sys}}$
20	329.0	$346.9 \pm 16.8_{\text{stat}} \pm 24.5_{\text{sys}}$
25	279.0	$295.6 \pm 15.6_{\text{stat}} \pm 20.9_{\text{sys}}$
30	243.0	$256.6 \pm 14.2_{\text{stat}} \pm 18.1_{\text{sys}}$
40	197.0	$199.5 \pm 11.8_{\text{stat}} \pm 14.1_{\text{sys}}$
50	159.0	$159.1 \pm 9.8_{\text{stat}} \pm 11.2_{\text{sys}}$
60	147.0	$129.5 \pm 8.3_{\text{stat}} \pm 9.1_{\text{sys}}$
80	120.0	$90.0 \pm 6.1_{\text{stat}} \pm 6.3_{\text{sys}}$
100	104.0	$65.9 \pm 4.6_{\text{stat}} \pm 4.7_{\text{sys}}$

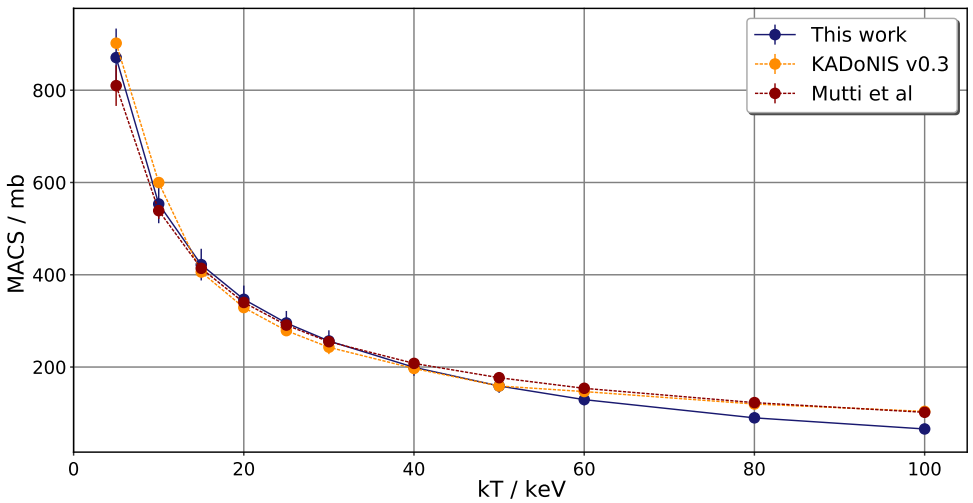

Fig. 7 Comparison of the MACS calculated in this work, KADoNIS v0.3 and Mutti et al. [27]

where $N_{b,x}$ is the number of events per energy bin and $N_{p,x}$ is the number of protons hitting the spallation target in the respective measurement. Furthermore the sample background from the steel sphere was subtracted from the spectrum by normalizing the measurement of the empty sphere to the ^{83}Kr spectrum. Here a strong 585 eV resonance from the steel sphere was chosen, that is also clearly visible in the ^{83}Kr measurement. Figure 5 shows the normalized spectra.

The resulting spectrum in combination with the neutron scatter correction (Sect. 4.2), the efficiency (Sect. 4.4) and the neutron flux correction (Sect. 4.1) allowed for the calculation of the energy dependent neutron capture cross section using Eq. 4.

$$\sigma_{^{83}\text{Kr},i} = \frac{k_{\text{BM}} \cdot C_{^{83}\text{Kr},i} \cdot f_{\text{sc},^{83}\text{Kr},i}}{\frac{C_{\text{BM},i}}{\sigma_{\text{BM},i}} \cdot N_{^{83}\text{Kr}} \cdot N_{\text{p}} \cdot \epsilon_{^{83}\text{Kr}}} \tag{4}$$

With i the respective energy bin, $C_{x,i}$ the events in either the ^{83}Kr or the background spectrum, $\sigma_{\text{BM},i}$ the cross section of the neutron monitor, $f_{\text{sc},^{83}\text{Kr},i}$ the scatter correction factor, N_p the number of protons and $\epsilon_{^{83}\text{Kr}}$ the ^{83}Kr efficiency. The number of atoms was calculated using Eq. 5.

$$N_{^{83}\text{Kr}} = \frac{m_{^{83}\text{Kr}} - m_{\text{sphere}}}{M_{^{83}\text{Kr}}} N_A = 1.83 \pm 0.02 \cdot 10^{20} \tag{5}$$

Here $m_{^{83}\text{Kr}}$ is the weight of the sphere with and m_{sphere} without ^{83}Kr. $M_{^{83}\text{Kr}}$ is the molar mass and N_A Avogadro constant. The resulting cross section is show in Fig. 6.

5.2 MACS

For the calculation of the astrophysically relevant MACS for ^{83}Kr Eq. 6 was used. Where i/j is the respective energy bin, E_i/E_j the corresponding energy in the middle of that bin and $\Delta E_i/\Delta E_j$ the bin width. As a result of the large uncertainties at an energy $E_n > 10^5$ eV, the evaluated cross section was used for this energy region. With a correction factor k_{MACS} from Eq. 7.

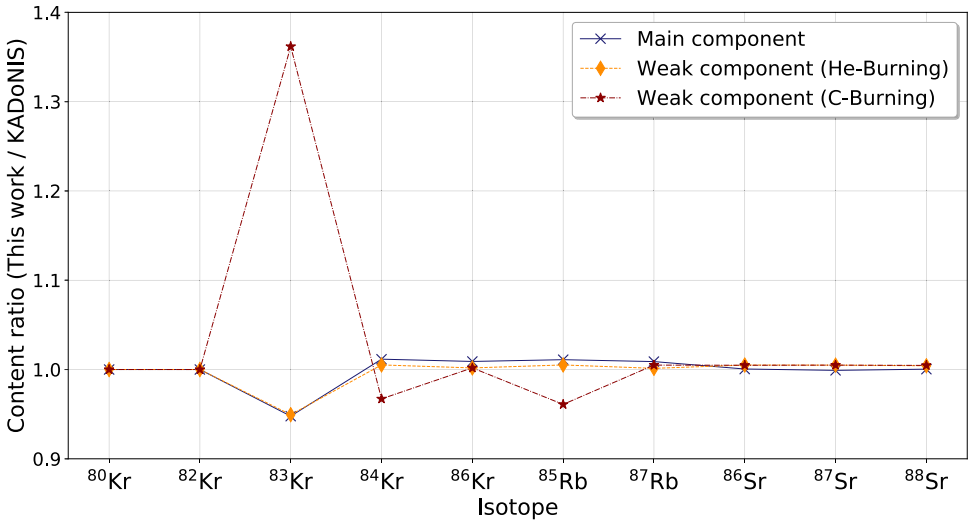

Fig. 8 Ratio of the abundances of the nucleosynthesis products calculated with NETZ

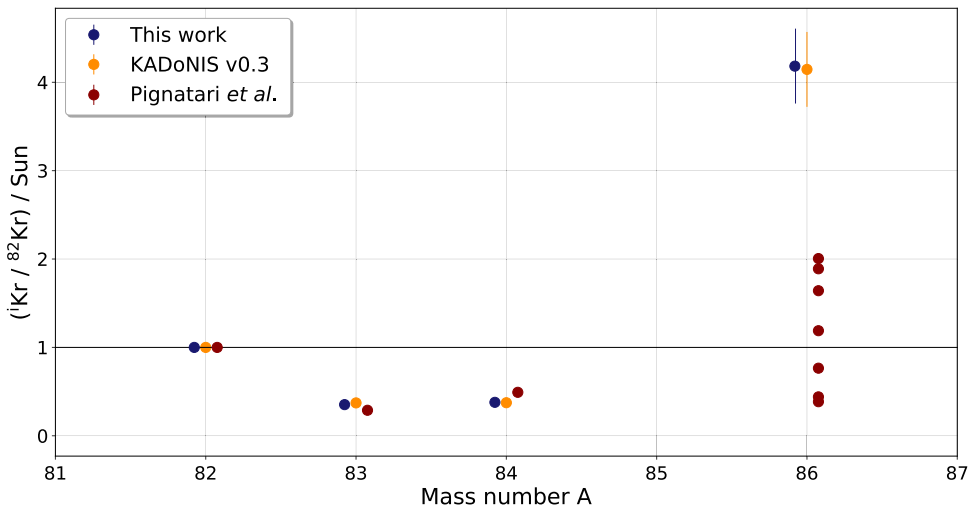

Fig. 9 Comparison of the NETZ simulations with Kr s-process abundances form SiC grains. Data from [32,33]

$$\mathrm{MACS}_{^{83}\mathrm{Kr}} = \left(\frac{4}{\pi}\right)^{1/2} \frac{1}{(kT)^2} \left(\sum_i \sigma(E_i) E_i \exp\left(-\frac{E_i}{kT}\right) \Delta E_i + \sum_j \sigma(E_j) E_j \exp\left(-\frac{E_j}{kT}\right) k_{\mathrm{MACS}} \Delta E_j \right). \quad (6)$$

$$k_{\mathrm{MACS}} = \frac{\sum_{25\ \mathrm{meV}}^{100\ \mathrm{meV}} f_{\mathrm{n,g;\ measurement}}}{\sum_{25\ \mathrm{meV}}^{100\ \mathrm{meV}} f_{\mathrm{n,g;\ ENDF}}} \quad (7)$$

The MACS at different energies from 5 to 100 keV in comparison to the KADoNIS v0.3 values are shown in Table 1 and Fig. 7.

5.3 NETZ

To examine the impact of the ^{83}Kr neutron capture cross sections measured in this work, sensitivity studies with the tool NETZ [23,28,29] were performed. NETZ simulates a reaction network depending on neutron density, temperature, and electron density, where several neutron induced reaction channels are taken into account, as well as α- and β-decays. The ratio of this work with KADoNIS v0.3 is shown in Fig. 8.

These simulations are the basis for a comparison of s-process abundances gained from SiC grains. Such grains develop in the outer regions of AGB stars when the outer envelope is rich in carbon due to convection [30]. An analysis for different Kr isotopes was done by Pignatari et al. [31]. Figure 9 shows a comparison with the NETZ simulations. For that purpose, the absolute abundances from NETZ were normalized to the abundance of ^{82}Kr which is a s-only isotope. In accordance to Pignatari the data was again normalized to the solar abundance. A good agreement for ^{83}Kr and ^{84}Kr can be observed. For ^{86}Kr the difference is much larger with a factor of 2–8.

6 Summary

The neutron capture cross section of ^{83}Kr was measured at the DANCE setup at the Los Alamos National laboratory. The new data is in good agreement with data from the KADoNIS v0.3 database. The impact of the cross section measured in this work was analysed using the NETZ code. These results were additionally compared with presolar grain distribution from Pignatari et al.

Acknowledgements The research leading to these results has received frunding from the European Research Council under the European Unions's Seventh Framework Programme (FP/2007-2013)/ERC Grant Agreement n. 615126. This work benefited from the use of the LANSCE accelerator facility at Los Alamos National Laboratory. M.K. acknowledges the support by Grant No. 23-06439S of the Czech Science Foundation. R.R. acknowledges the generous support by the Glynn family. We would also like to express our gratitude to the anonymous referees for the extremely valuable comments and careful reading.

Funding Open Access funding enabled and organized by Projekt DEAL.

Data availability This manuscript has associated data in a data repository. [Authors' comment: The data will be made available through the EXFOR database.]

References

1. R. Reifarth, C. Lederer, F. Käppeler, Neutron reactions in astrophysics. J. Phys. G: Nucl. Phys. **41**(5), 053101 (2014)
2. A. Arcones, F.-K. Thielemann, Neutrino-driven wind simulations and nucleosynthesis of heavy elements. J. Phys. G: Nucl. Part. Phys. **40**(1), 013201 (2013)
3. M. Pignatari, K. Göbel, R. Reifarth, C. Travaglio, The production of proton-rich isotopes beyond iron: the γ-process in stars. Int. J. Modern Phys. E **25**(4), 1630003 (2016)
4. K. Göbel, J. Glorius, A. Koloczek, M. Pignatari, R. Reifarth, R. Schach, K. Sonnabend, Nucleosynthesis simulations for the production of the p-nuclei ^{92}Mo and ^{94}Mo in a Supernova type II model. EPJ Web Conf. **93**, 03006 (2015). https://doi.org/10.1051/epjconf/20159303006
5. R. Reifarth, K. Göbel, p-process fluxes. https://exp-astro.de/fluxes/ (2020)
6. M. Schwarzschild, R. Härm, Thermal instability in non-degenerate stars. Astrophys. J. **142**, 855 (1965). https://doi.org/10.1086/148358
7. C. Arlandini, F. Käppeler, K. Wisshak, R. Gallino, M. Lugaro, M. Busso, O. Straniero, Neutron capture in low mass asymptotic giant branch stars: cross sections and abundance signatures. Astrophys. J. **525**, 886–900 (1999)
8. R. Reifarth, C. Arlandini, M. Heil, F. Käppeler, P.V. Sedychev, A. Mengoni, M. Herman, T. Rauscher, R. Gallino, C. Travaglio, Stellar neutron capture on promethium - implications for the *s*-process neutron density. Astrophys. J. **582**, 1251 (2003)
9. R. Reifarth, F. Käppeler, F. Voss, K. Wisshak, R. Gallino, M. Pignatari, O. Straniero, ^{128}Xe and ^{130}Xe: testing he-shell burning in asymptotic giant branch stars. Astrophys. J. **614**, 363 (2004). https://doi.org/10.1086/422206
10. R. Reifarth, S. Dababneh, S. Fiebiger, J. Glorius, K. Göbel, M. Heil, P. Hillmann, T. Heftrich, C. Langer, O. Meusel, R. Plag, S. Schmidt, Z. Slavkovská, D. Veltum, M. Weigand, C. Wiesner, C., Wolf, A. Zadeh, Nuclear astrophysics at FRANZ. J. Phys. Conf. Ser. **940**, 012024 (2018). https://doi.org/10.1088/1742-6596/940/1/012024
11. R. Reifarth, T.A. Bredeweg, A. Alpizar-Vicente, J.C. Browne, E.-I. Esch, U. Greife, R.C. Haight, R. Hatarik, A. Kronenberg, J.M. O'Donnell, R.S. Rundberg, J.L. Ullmann, D.J. Vieira, J.B. Wilhelmy, J.M. Wouters, Background identification and suppression for the measurement of (n,γ) reactions with the dance array at lansce. Nucl. Instrum. Method. A **531**, 530 (2004)
12. G. Rupp, D. Petrich, F. Käppeler, J. Kaltenbaek, B. Leugers, R. Reifarth, High pressure gas spheres for neutron and photon experiments. Nucl. Instrum. Methods A **608**, 152 (2009)
13. Data sheet Isoflex USA. 03.06.15
14. P.W. Lisowski, C.D. Bowman, G.J. Russell, S.A. Wender, The Los Alamos national laboratory spallation neutron sources. Nucl. Sci. Eng. **106**, 208 (1990)
15. P.W. Lisowski, K.F. Schoenberg, The Los Alamos neutron science center. Nucl. Instrum. Methods Phys. Res. Sect. A **562**(2), 910–914 (2006)
16. M. Mocko, G. Muhrer, Fourth-generation spallation neutron target-moderator-reflector-shield assembly at the Manuel Lujan Jr. neutron scattering center. Nucl. Instrum. Methods Phys. Res. Sect. A **704**, 27–35 (2013)
17. R. Reifarth, P. Erbacher, S. Fiebiger, K. Göbel, T. Heftrich, M. Heil, F. Käppeler, N. Klapper, D. Kurtulgil, C. Langer, C. Lederer-Woods, A. Mengoni, B. Thomas, S. Schmidt, M. Weigand, M. Wiescher, Neutron-induced cross sections - from raw data to astrophysical rates. Eur. Phys. J. Plus **133**, 424 (2018)
18. R. Reifarth, E.-I. Esch, A. Alpizar-Vicente, E.M. Bond, T.A. Bredeweg, S.E. Glover, U. Greife, R. Hatarik, R.C. Haight, A. Kronenberg, J.M. O'Donnell, R.S. Rundberg, J.M. Schwantes, J.L. Ullmann, D.J. Vieira, J.B. Wilhelmy, J.M. Wouters, (n, γ) measurements on radioactive isotopes with DANCE. Nucl. Instrum. Methods Phys. Res. Sect. B **241**(1), 176–179 (2005)
19. M. Heil, R. Reifarth, M.M. Fowler, R.C. Haight, F. Käppeler, R.S. Rundberg, E.H. Seabury, J.L. Ullmann, J.B. Wilhelmy, K. Wisshak, F. Voss, A 4π baf$_2$ detector for (n,γ) cross-section measurements at a spallation neutron source. Nucl. Instrum. Method A **459**, 229 (2001)
20. M.B. Chadwick, M. Herman, P. Obložinský, M.E. Dunn, Y. Danon, A.C. Kahler, D.L. Smith, B. Pritychenko, G. Arbanas, R. Arcilla, R. Brewer, D.A. Brown, R. Capote, A.D. Carlson, Y.S. Cho, H. Derrien, K. Guber, G.M. Hale, S. Hoblit, S. Holloway, T.D. Johnson, T. Kawano, B.C. Kiedrowski, H. Kim, S. Kunieda, N.M. Larson, L. Leal, J.P. Lestone, R.C. Little, E.A. McCutchan, R.E. MacFarlane, M. MacInnes, C.M. Mattoon, R.D. McKnight, S.F. Mughabghab, G.P.A. Nobre, G. Palmiotti, A. Palumbo, M.T. Pigni, V.G. Pronyaev, R.O. Sayer, A.A. Sonzogni, N.C. Summers, P. Talou, I.J. Thompson, A. Trkov, R.L. Vogt, S.C. van der Marck, A. Wallner, M.C. White, D. Wiarda, P.G. Young, ENDF/B-VII.1 Nuclear data for science and technology: cross sections, covari-

ances, fission product yields and decay data. Nucl. Data Sheets **112**, 2887–2996 (2011)
21. J. Apostolakis, Cern program library long writeup, w5013. Technical report, CERN, GEANT library (1993). http://wwwinfo.cern.ch/asd/geant/
22. R. Reifarth, M. Heil, F. Käppeler, F. Voss, K. Wisshak, R.C. Haight, M.R. Dragowsky, M.M. Fowler, R.S. Rundberg, J.L. Ullmann, J.B. Wilhelmy, E.H. Seabury, New Geant Simulations of Neutron Capture Experiments with a 4π baf$_2$ Detector. Technical report, Report LA-UR-01-4185, Los Alamos National Laboratory (2001)
23. M. Weigand, T.A. Bredeweg, A. Couture, K. Göbel, T. Heftrich, M. Jandel, F. Käppeler, C. Lederer, N. Kivel, G. Korschinek, M. Krtička, J.M. O'Donnell, J. Ostermöller, R. Plag, R. Reifarth, D. Schumann, J.L. Ullmann, A. Wallner, ^{63}Ni (n,γ) cross sections measured with DANCE. Phys. Rev. C **92**(4), 045810 (2015)
24. F. Bečvář, Simulation of γ cascades in complex nuclei with emphasis on assessment of uncertainties of cascade-related quantities. Nucl. Instrum. Method A **417**, 434 (1998)
25. J. Kopecky, M. Uhl, Test of gamma-ray strength functions in nuclear reaction model calculations. Phys. Rev. C **41**(5), 1941 (1990)
26. D. Abriola, M. Bostan, S. Erturk, M. Fadil, M. Galan, S. Juutinen, T. Kibédi, F. Kondev, A. Luca, A. Negret, Nuclear data sheets for A= 84. Nucl. Data Sheets **110**(11), 2815–2944 (2009)
27. P. Mutti, H. Beer, A. Brusegan, F. Corvi, R. Gallino, New Kr cross sections and astrophysical constraints on presolar grains. In: AIP Conference Proceedings, vol. 769, pp. 1327–1330 (2005). AIP
28. S. Jaag, NETZ - internal report 14.01.01/p35g. Technical report, Forschungszentrum Karlsruhe (1991)
29. R. Reifarth, J. Ostermöller, R. Plag, M. Weigand, NETZ - Simulating s-process nucleosynthesis. https://exp-astro.de/netz/ (2020)
30. E. Zinner, stellar nucleosynthesis and the isotopic composition of presolar grains from primitive meteorites. Ann. Rev. Earth Planet. Sci. **26**, 147–188 (1998)
31. M. Pignatari, R. Gallino, S. Amari, A.M. Davis, Krypton in presolar mainstream SiC grains from AGB stars. Memorie della Societa Astronomica Italiana **77**, 897 (2006)
32. R.S. Lewis, S. Amari, E. Anders, Interstellar grains in meteorites II. SiC and its noble gases. Geochimica et Cosmochimica Acta **58**(1), 471–494 (1994)
33. K. Lodders, H. Palme, H.-P. Gail, Abundances of the elements in the solar system. Landolt Börnstein **4B**, 712 (2009) arXiv:0901.1149 [astro-ph.EP]. https://doi.org/10.1007/978-3-540-88055-4_34